Journal of Power Sources 201 (2012) 259–266

Contents lists available at SciVerse ScienceDirect

Journal of Power Sources

journal homepage: www.elsevier.com/locate/jpowsour

Few-layer SnS_2/graphene hybrid with exceptional electrochemical performance as lithium-ion battery anode

Kun Chang [a], Zhen Wang [a], Guochuang Huang [a], He Li [a], Weixiang Chen [a,*], Jim Yang Lee [b]

[a] Department of Chemistry, Zhejiang University, Hangzhou 310027, PR China
[b] Department of Chemical and Biomolecular Engineering, National University of Singapore, 10 Kent Ridge Crescent, 119260 Singapore, Singapore

ARTICLE INFO

Article history:
Received 3 October 2011
Received in revised form 25 October 2011
Accepted 27 October 2011
Available online 6 November 2011

Keywords:
Few-layer
Solution-phase
Tin disulfide/graphene hybrid
Defect sites
Lithium ion battery
Anode material

ABSTRACT

Here we develop a facile process for preparing few-layer SnS_2/graphene (FL-SnS_2/G) hybrid by solution-phase method employing L-cysteine as a complexing, sulfide source and reducing agent. The FL-SnS_2/G hybrid is characterized by XRD, SEM and HRTEM. It is demonstrated that the few-layer SnS_2 with defects or disorder structure supports on graphene surface. Electrochemical tests show the FL-SnS_2/G hybrid exhibits an extraordinary capacity of up to 920 mAh g^{-1} with excellent cycling stability and high-rate capability. The significant improvement in the electrochemical performances is attributed to the robust composite structure and some synergistic interactions between few-layer SnS_2 and graphene. Electrochemical impedance spectra confirm that the incorporation of graphene considerably improved the electric conductivity and electron rapid transfer of the FL-SnS_2/G hybrid. Therefore, this new kind of FL-SnS_2/G hybrid can be used as a promising anode material for lithium ion batteries.

1. Introduction

Li-ion batteries (LIBs) are currently the most advanced rechargeable batteries for consumer electronic products. However, their specific capacity, energy and power densities, and cycle life have to be continually improved to meet new and more demanding applications such as electric vehicle (EV) propulsion and distributed power generation. Such improvements are best achieved through materials innovations. The anode material is of particular interest since it has an overriding influence on LIB the performances. Graphite, the most ubiquitous anode material for the LIBs today, should be replaced by alternatives which can increase the anode specific capacity beyond the theoretical limit of 372 mAh g^{-1} [1]. The discovery of graphene nanosheets, or single layers of graphite, with nearly double the specific capacity of graphite, has raised the prospect for the replacement of the graphite anode [2–7]. The specific capacity can also be further increased by compositing graphene with semi-metals or metal oxides (*e.g.* Sn, Si, SnO_2) with high Li storage capacities but are not effective Li hosts on their own because of inadequate electrical conductivities. Many of these composites have shown higher specific capacities and improvements in the cyclability of SnO_2, Sn and Si nanomaterials for Li storage [8,9]. The cycle stability of these composites, however, is still not satisfactory and ~15–30% of capacity loss is typical after 30–50 cycles [10–12]. The unsatisfactory cycle stability was probably caused by structural and morphological mismatches between graphene and Sn, Si and metal oxides.

SnS_2 has a layered CdI_2-type structure with tin atoms sandwiched between two layers of hexagonal close-packed sulfur atoms [13,14]. The spacious configuration is more tolerant of cycling-induced volume excursions and enhances the accessibility of the Li host; both of which should contribute to high capacity and improved cycling stability [15,16]. While high capacity has been demonstrated, for example in the work of Seo et al. [17] where two-dimensional SnS_2 nanoplates prepared from the thermal decomposition of $Sn(S_2CNEt_2)_4$ showed an initial high capacity of 645 mAh g^{-1}. The capacity loss was ~15% after 30 cycles. Ultrathin hexagonal SnS_2 nanosheets could also be prepared by the hydrothermal reaction between $SnCl_4$ and thioacetamide [18]. The lithium storage capacity was slightly lower, at 513 mAh g^{-1}, but it cycled well at the current density of 100 mA g^{-1}. However, the nanosheets were not tested at higher current densities which are of more interest to large scale application such full and/or hybrid EVs. In view of the low intrinsic conductivity of SnS_2, it is unlikely that the SnS_2 nanosheets alone can meet the high rate requirements of these demanding applications.

Since SnS_2 is structurally and morphologically analogous to graphene, it is more compatible with graphene for the preparation of a nanocomposite than previous graphene composites with morphologically and structurally dissimilar materials such as Sn,

* Corresponding author. Tel.: +86 571 87952477; fax: +86 571 87951895.
E-mail address: weixiangchen@zju.edu.cn (W. Chen).

0378-7753/$ – see front matter © 2011 Elsevier B.V. All rights reserved.
doi:10.1016/j.jpowsour.2011.10.132

Si and SnO_2. We will demonstrate the design and the synthesis of a new LIB anode material in the form of few-layer SnS_2/graphene (FL-SnS_2/G) hybrid. This particular combination leverages on the complementarity and structural similarity between the two constituents to create a robust microarchitecture and to enhance the synergistic interactions between FL-SnS_2 and graphene. Graphene with high conductivity can ensure an overall high conductivity for the FL-SnS_2/G hybrid. In addition, the extensively delocalized π-conjugation system of graphene could interact with the outer electrons of the S atoms in the SnS_2 nanosheets to support fast charge transfer in the electrode reaction [19]. Hence the FL-SnS_2/G hybrid can in principle have high specific capacity, good cycle stability and high-rate performance all in one. To the best of our knowledge at the time of writing, the FL-SnS_2/G hybrid is totally new and has not been reported before.

A facile L-cysteine-assisted solution-chemistry method was used for the preparation of the FL-SnS_2/G hybrid with the molar ratio of 1:2. Evaluations of electrochemical properties for reversible Li^+ storage showed very high specific capacities up to 920 mAh g^{-1} as well as excellent rate capability and cycle stability. The novel FL-SnS_2/G hybrid therefore has great potential as a LIB anode material for demanding applications.

2. Experimental

2.1. Synthesis of graphene oxide (GO)

Natural graphite powder (Shanghai Colloid Chemical Plant, China) was oxidized to graphite oxide by the modified Hummers method. Specifically graphite powder (0.04 g) was dispersed in 50 ml concentrated H_2SO_4 in an ice bath. 3.0 g $KMnO_4$ was then added gradually. The mixture was stirred for 2 h and then diluted with deionized water. 10 ml of 30% H_2O_2 was then added to the solution until the color of the mixture changed to bright yellow. The graphite oxide (GO) prepared as such was re-dispersed in deionized water and then exfoliated to GO sheets by ultrasonication. A brown homogeneous supernatant was obtained by the repeated centrifuging and washing.

2.2. Synthesis of few-layer SnS_2/graphene

0.480 g L-cysteine (L-cys) was dissolved in 40 ml deionized water and then 0.350 g $SnCl_4{\cdot}5H_2O$ was added with stirring until it was completely dissolved. The GO suspension prepared above was added to the mixture followed by 40 ml deionized water. After ultrasonication and stirring for 30 min, the mixture was transferred to a 100 ml Teflon-lined stainless steel autoclave, sealed tightly, and heated at 180 °C for 12 h. After cooling to room temperature naturally, a black precipitate was collected by centrifugation, washed with deionized water and ethanol, and then dried in a vacuum oven at 80 °C for 24 h. In control experiment, the layered SnS_2 was also prepared by the above same procedure without the presence of GO nanosheets.

2.3. Characterizations

Samples were characterized with X-ray diffraction (XRD; Thermo X'TRA X-ray diffractometer with Cu Kα-source), high-resolution transmission electron microscopy (HRTEM; JEOL JEM-2010, 200 kV), and field emission scanning electron microscopy (FESEM; SIRION-100), and energy dispersive X-ray spectroscopy (EDX, GENENIS-4000).

2.4. Electrochemical measurements

Electrochemical measurements were carried out using two-electrode cells assembled in an argon-filled glove box. Li sheets were used as the counter *cum* reference electrode, and a polypropylene film (Celgard-2300) was used as the separator. The electrolyte was a 1.0 M $LiPF_6$ solution in a mixture of ethylene carbonate/dimethyl carbonate (1:1 by volume). The working electrodes were prepared by a slurry coating procedure. The slurry contained 85 wt.% active material (FL-SnS_2/G or SnS_2), 5 wt.% carbon black and 10 wt.% polyvinyldifluoride (PVDF) in *N*-methyl-2-pyrrolidinone solvent. The obtained slurry was spread on a copper foil with 14 mm in diameter and 0.02 mm in thickness, dried at 110 °C for 12 h in vacuum and then pressed. Galvanostatic charging and discharging were carried out on a CBT-138-320 battery tester between 0.01 and 1.5 V at the current densities sated in the paper. Cyclic voltammetric measurements were performed on an electrochemical workstation (Zahner IM6ex) in the potential range of 0.01–3.00 V *vs.* Li/Li^+ using a scan rate of 0.5 mV s^{-1}. Electrochemical impendence spectra (EIS, PARSTAR 2273) were obtained by applying a sine wave with amplitude of 5.0 mV over the frequency range from 200 kHz to 0.01 Hz.

3. Results and discussion

The L-cysteine-assisted synthesis of layered SnS_2 and FL-SnS_2/G hybrid is shown schematically in Scheme 1. In a typical procedure, graphite powder was first converted to graphene oxide (GO) by the Hummers method [20]. L-Cysteine (L-cys) was dissolved in deionized water, to which $SnCl_4{\cdot}5H_2O$ was added. Sn^{4+} ions can be easily complexed with L-cys because of the affinity provided by the sulfur group. The Sn (IV) solution and the as-prepared GO were fully mixed and treated under hydrothermal conditions at 180 °C for 12 h to form a uniform distribution of the layered SnS_2 on graphene sheets. It is hypothesized that the Sn^{4+}-L-cys complex was adsorbed on the GO surface and formed the FL-SnS_2/G hybrid under hydrothermal conditions. The layered SnS_2 grown as such were anchored to the graphene surface possibly through the abundance of functional groups on the surface of the GO sheets, such as hydroxyl, carboxyl, and epoxy groups [21].

In a control experiment, we also synthesized the layered SnS_2 and graphene nanosheets (GNS) by L-cys-assisted solution-chemistry method at 180 °C for 12 h. Fig. 1 shows the SEM images of the layered SnS_2, FL-SnS_2/G hybrid and graphene. It can be found from Fig. 1a and b that the SnS_2 shows a large-scaled sheet structure with the diameter of ~1 μm, which mainly depends on the layered crystal structure itself. As shown in Fig. 1f, the as-prepared GO sheets can be reduced to graphene by H_2S in situ released from L-cys during the hydrothermal process, and the reduced GO sheets can be easily restacked under the hydrothermal condition (Fig. 1g). However, the FL-SnS_2/G hybrid sports a three-dimensional (3D) architecture consisted of the curved nanosheets (Fig. 1c–e). According to the view of Shi et al. [22], the self-assembly of graphene into a 3D structures can be attributed to the partial overlap or coalescence of flexible graphene sheets during the hydrothermal process. In this work, the self-assembly was promoted under the L-cys-assisted hydrothermal conditions but the different self-assembly elements (layered SnS_2 and graphene) were involved depending on their interactions. As the anode materials of LIBs, this 3D architecture of the FL-SnS_2/G hybrid with the rough surface can increase the interfacial areas between electrolyte/electrode and thus improve lithium ions diffusion.

The XRD pattern in Fig. 2a shows that the layered SnS_2 exhibits very sharp diffraction peaks, which could all be indexed to hexagonal SnS_2 (JCPDS Card No. 23-0677). The very sharp diffraction peaks, especially for (0 0 1) plane of the SnS_2, indicates that the

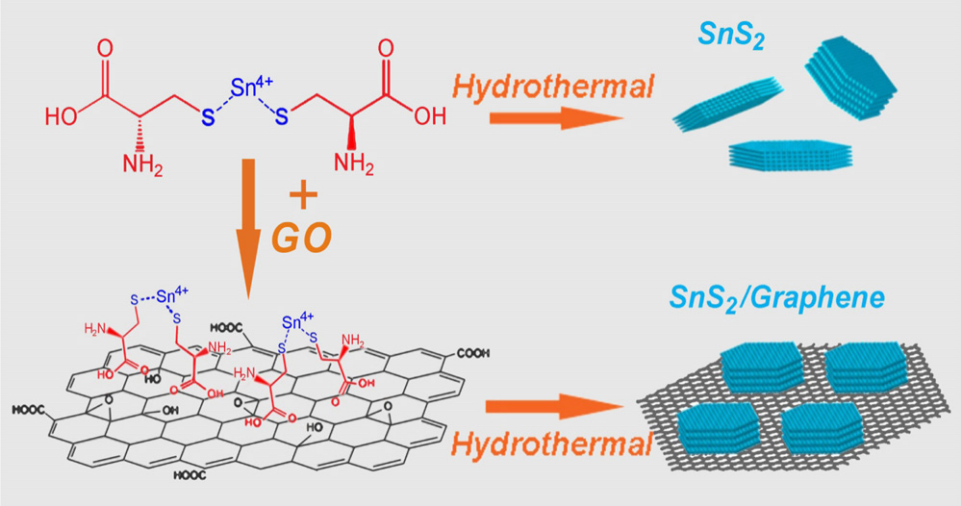

Scheme 1. Schematic of L-cys-assisted synthesis of the layered SnS_2 and FL-SnS_2/G hybrid by the solution-phased method.

SnS_2 prepared by this method possess high crystallinity with well-layered structure. Fig. 2b shows that the FL-SnS_2/G hybrid also displayed the same SnS_2 diffraction peaks except for the (0 0 1) peak at $2\theta = 15.1^\circ$, the intensity of which was much lower than in the case of layered SnS_2, and the width of which was larger than that of layered SnS_2, indicating that growth of the layered SnS_2 (0 0 1) plane was inhibited in the hybrid due to the intervention of graphene. According to the Scherrer equation ($D = K\lambda/\beta\cos\theta$),

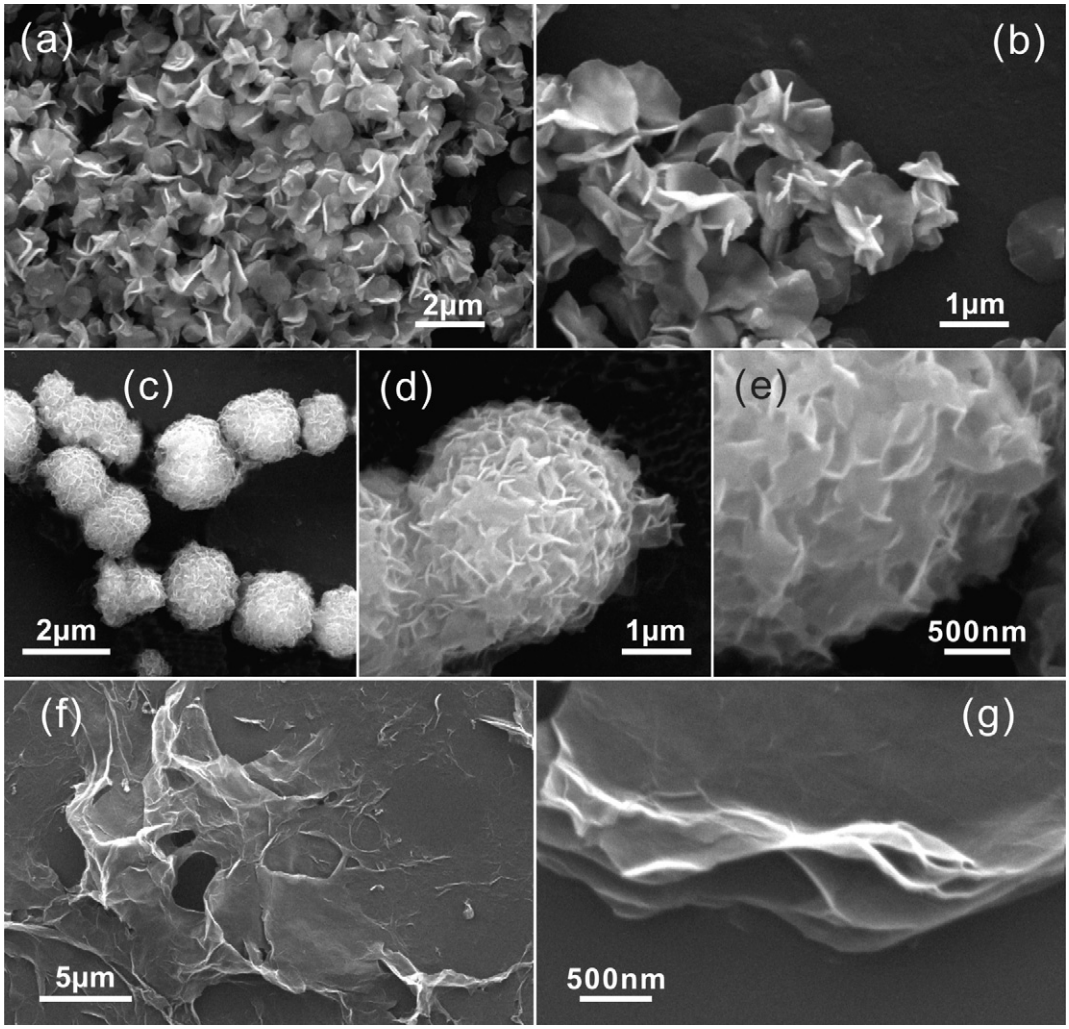

Fig. 1. SEM images of different kinds of samples: (a) and (b) for the layered SnS_2 obtained by hydrothermal route at 180 °C for 12 h; (c–e) for FL-SnS_2/G hybrid synthesized by purposed method; (f) and (g) for graphene reduced from GO sheets by L-cys-assisted solution-chemistry method at 180 °C for 12 h.

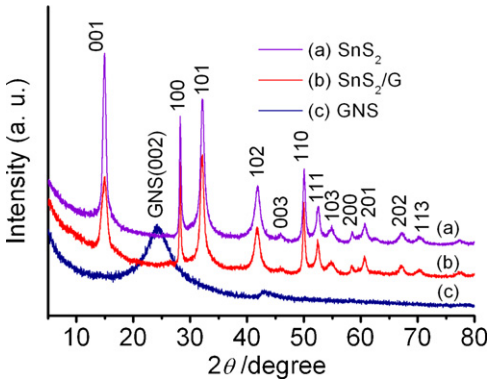

Fig. 2. XRD patterns of (a) the layered SnS_2, (b) FL-SnS_2/G hybrid, and (c) graphene nanosheets prepared by L-cys-assisted solution-chemistry method.

the average *c*-stacking height, calculated from the (0 0 1) reflection, was 15.3 nm for layered SnS_2 and 4.7 nm for FL-SnS_2/G hybrid. Therefore, we could reasonably estimate that the average layer number of SnS_2 was about 26 layers and that of FL-SnS_2 in the hybrid was about 8 layers according to the interlayer distance of the (0 0 1) plane of 0.59 nm. Fig. 2c shows a broad diffraction peak at $2\theta = 24.1^\circ$ which is assignable to the (0 0 2) plane of GNS [23,24]. This peak indicates that the restacking of graphene monolayers occurred in the hydrothermal process. According to Bragg equation, it could be calculated that the interlayer distance of GNS (*d*-spacing of 0 0 2 plane) is 0.37 nm, which was slightly larger than that of graphite ($2\theta = 26.3^\circ$) with 0.33 nm. However, there was no GNS (0 0 2) peak in the XRD spectrum of the FL-SnS_2/G hybrid, indicating that the graphene sheets did not undergo restacking in the hybrid. The fact was attributed to that the FL-SnS_2 sheets formed in situ were supported on the graphene surface and in turn prevented the restacking of the graphene layers during the hydrothermal process.

In order to reveal the fine microstructure, the layered SnS_2 and FL-SnS_2/G hybrid were characterized by TEM and HRTEM. As shown in Fig. 3a and b, the layered SnS_2 shows a well-layered structure stacked tens (about 24) of SnS_2 layers by weak Van der Waals interaction with an interlayer distance of the (0 0 1) plane of 0.59 nm, which is agree the XRD analysis as shown in Fig. 2a. Fig. 3c and d further shows that the layered SnS_2 with few layers supports on graphene surface. Fig. 3d clearly shows that the SnS_2 on the graphene ranges from 5 to 12 layers with defects or disorder structure. During the hydrothermal process, GO sheets could be reduced to graphene by H_2S in situ released from L-cys. GO and reduced GO sheets served as the substrate for the nucleation and growth of SnS_2 into a layered structure due to the interaction between the functional group of GO or reduced GO surface and Sn precursors. On another hand, the intervention of graphene disturbs the well-growth of SnS_2 layered crystal structure, especially in (0 0 1) plane of SnS_2, resulting in formation of the few-layer SnS_2 with defects or disorder structures on graphene surface. Xiao et al. [25] believed that the defects or disorder structures of exfoliated MoS_2 sheets facilitated more lithium ions insertion and improved their lithiation capacity. Therefore, the defects or disorder structures of the few-layer SnS_2 support on the graphene have some positive effects on the improvement in the electrochemical performances of FL-SnS_2/G hybrid as LIB anode material.

The evaluation of electrochemical properties of the FL-SnS_2/G hybrid as Li-ion battery anode was performed in a two-electrode cell. Fig. 4a and b compares the charge and discharge characteristics of the layered SnS_2 and FL-SnS_2/G hybrid electrodes between 0.01 and 1.5 V *vs.* Li^+/Li at a current density of 100 mA g^{-1}. In the first discharge (lithiation) cycle, an inconspicuous potential plateau appeared at 1.8 V which can be attributed to the formation of Li_xSnS_2 when lithium ions were intercalated into the SnS_2 layers to some extent without causing phase decomposition [26,27]. The irreversible plateau that emerged at about 1.2 V can be assigned to the decomposition of SnS_2 to Sn and Li_2S [28]. In the potential range of 0.01–0.5 V, lithium ions alloyed with the Sn metal, form a series of Li–Sn alloys. For the subsequent cycles, charge and discharge plateaus were detected in the 0.5–0.7 V and 0.5–0.01 V *vs.* Li^+/Li potential regions. To further reveal the lithiation mechanism, the in situ XRD of SnS_2 and FL-SnS_2/G electrodes at the end of first discharge (lithiation) are shown in Fig. 5. From the in situ XRD patterns, it can be seen that no characteristic diffraction peaks of SnS_2 can be found (comparing with Fig. 2). On the contrary, it can be indexed that Li_2S, LiC_6, Li and Li_xSn are observed, in which Li_xSn is mainly consisted by $Li_{3.5}Sn$ at $2\theta = 21.6^\circ$. In our previous work [29], we indicated that some oxygen-functionalized groups could be reduced during the first discharge at about 2.0 V. While there are a small number of oxygen-functionalized groups in the reduced graphene oxide, it is not found the diffraction peaks of Li_2O in Fig. 5, indicating such a small number of oxygen-functionalized groups in the FL-SnS_2/G hybrid cannot affect the capacity of final product.

Fig. 4a and b also shows that the capacities from the first discharge and charge (delithiation) cycles were 1309 and 462 mAh g^{-1} for the layered SnS_2 electrode, and 1664 and 705 mAh g^{-1} for the FL-SnS_2/G hybrid electrode respectively. These initial capacity losses could come from incomplete conversion reaction [30] and the irreversible loss of lithium ions due to the formation of a solid electrolyte interphase layer (SEI). Besides, during the charge/discharge process, the fractions of lithium ions are trapped in the nanoclusters or defect sites and hardly exfoliated, inducing irreversible capacity. While the FL-SnS_2/G hybrid delivers a low coulombic efficiency of 42.4% at 1st cycle, it is still larger than that of other reports (about ~30% at 1st cycle for pure SnS_2) [27,31,32]. In our previous work, we attributed this factor to graphene is facilitating Li^+ ions extraction [33]. Fig. 4c shows the cycling performance of the layered SnS_2 and FL-SnS_2/G hybrid electrodes at the current density of 100 mA g^{-1}. The layered SnS_2 clearly experienced a huge reduction in capacity with cycling: from 462 mAh g^{-1} initially to 163 mAh g^{-1} after 50 cycles with a low capacity retention rate of 35.3%. On the contrary, the FL-SnS_2/G hybrid electrode displayed a maximum reversible capacity of 920 mAh g^{-1} which did not diminish with cycling in the same number of cycles. Not only is the cycle stability of the FL-SnS_2/G hybrid exceptional, the reversible specific capacity of the FL-SnS_2/G hybrid at 920 mAh g^{-1} is also the previous record for carbon-coated SnS_2 material (~700 mAh g^{-1}) [26]. In addition to the high reversible capacity and exceptional cycle stability, the FL-SnS_2/G hybrid also demonstrated excellent rate capability (Fig. 4d). Even with a 10-fold increase in current density to 1000 mA g^{-1}, the specific capacity was still an impressively high 600 mAh g^{-1}; a remarkable improvement over the performance of SnS_2 nanosheets at a current density of 100 mA g^{-1} (~520 mAh g^{-1}). Whereas, the layered SnS_2 delivers the reversible capacity of only 220–200 mAh g^{-1} at a current density of 1000 mA g^{-1}, as shown in Fig. 4d, exhibiting a poor rate capability. In addition, the good cycle stability at 100 mA g^{-1} was also replicated at other current densities: the specific capacity of the hybrid immediately returned to 920 mAh g^{-1} (and remained unchanged in subsequent cycles) even after the FL-SnS_2/G hybrid was cycled at different current densities in the 100–1000 mA g^{-1} current range (Fig. 4d). These experiential results indicate the usability of the FL-SnS_2/G hybrid even for high rate applications (current density ~1000 mA g^{-1}).

For comparison, we also present the electrochemical results of pure graphene. Fig. 6 shows the charge and discharge characteristics of graphene electrode between 0.01 and 3.0 V *vs.* Li^+/Li at a current density of 100 mA g^{-1}. As shown in Fig. 6a, the GNS electrode delivers an initial reversible capacity of 887 mAh g^{-1} at the

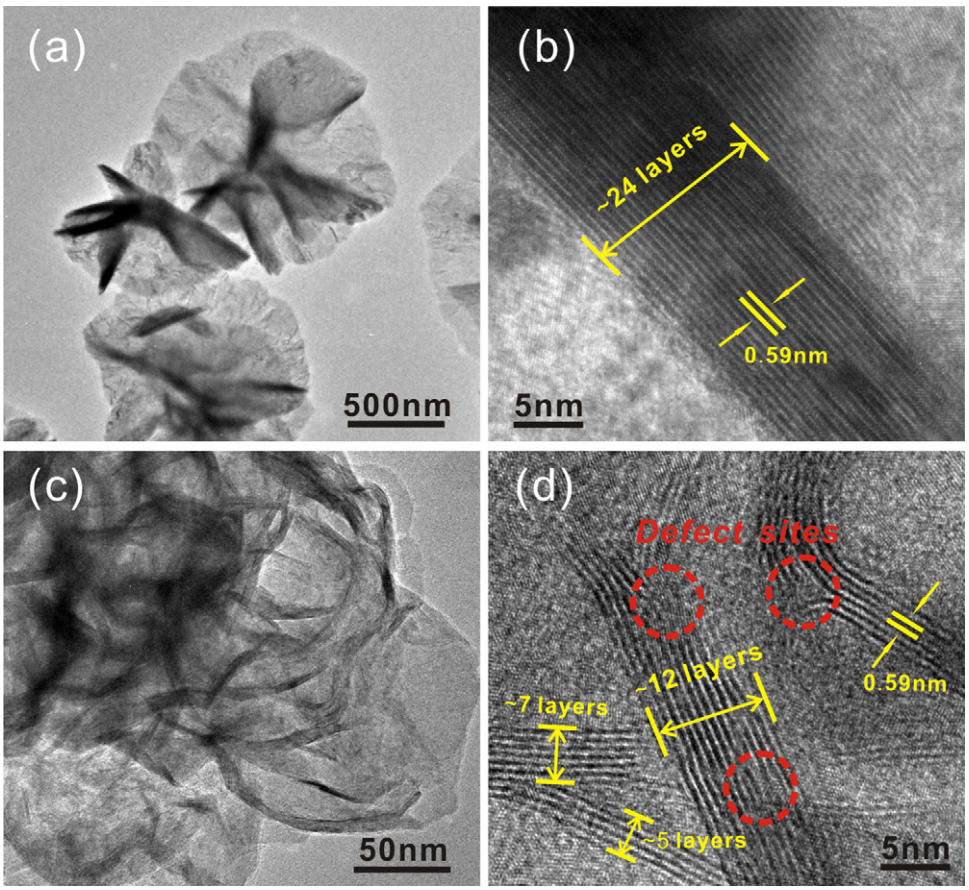

Fig. 3. Microstructure of the layered SnS_2 and FL-SnS_2/G hybrid by L-cysteine-assisted solution-chemistry method: (a) and (b) is the TEM and HRTEM images of the layered SnS_2 respectively, (c) and (d) is the TEM and HRTEM images of FL-SnS_2/G hybrid respectively.

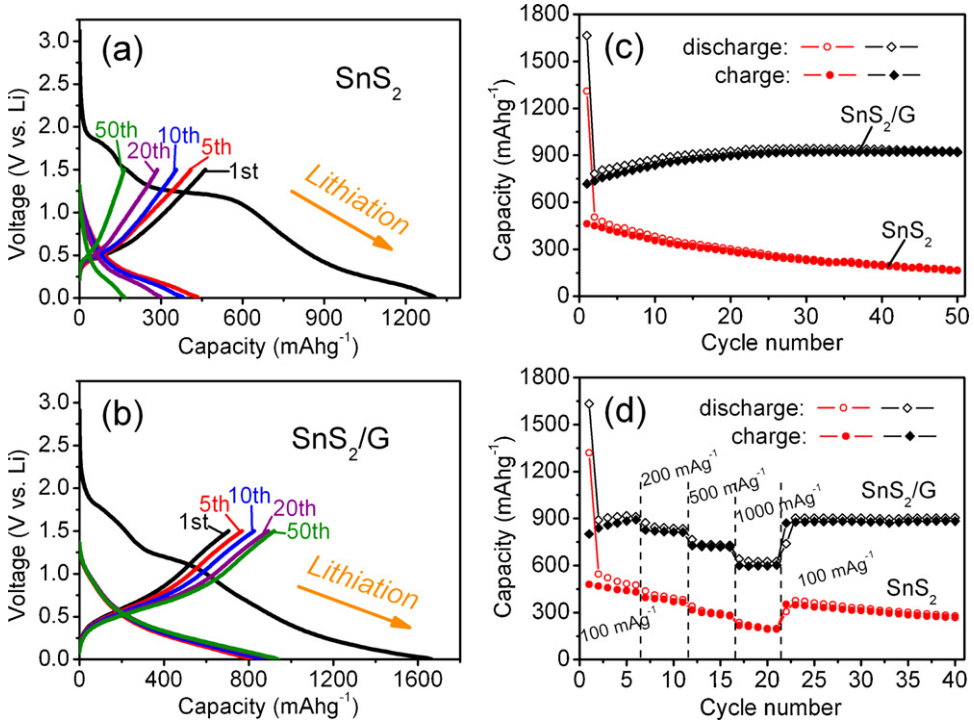

Fig. 4. Charge and discharge curves of (a) layered SnS_2 and (b) FL-SnS_2/G hybrid at a current density of 100 mA g^{-1}; (c) cyclic behavior of the SnS_2 and FL-SnS_2/G electrodes at a current density of 100 mA g^{-1}; (d) rate performance of FL-SnS_2/G at different current densities.

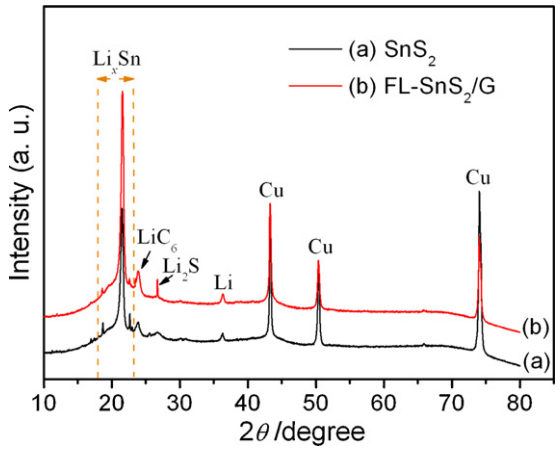

Fig. 5. In situ XRD patterns of (a) layered SnS_2 and (b) FL-SnS_2/G hybrid after 1st discharge from the initial potential to 0.005 V at a current density of 100 mA g^{-1}.

first cycle. If taking the charging/discharging potential region into account, the initial reversible capacity of the GNS electrode is about 390 mAh g^{-1} at 0.01–1.5 V *vs.* Li^+/Li, which is much lower than that of FL-SnS_2/G hybrid. Fig. 6b shows that the GNS remains the capacity of 600 mAh g^{-1} after 50 cycles, which is also much lower than that of SnS_2/G hybrid after 50 cycles. According to the analysis of EDAX (as shown in Table 1), the FL-SnS_2/G hybrid contain Sn, S, C and a small number of O, which comes from a few parts of the graphene that were not completely reduced during the hydrothermal process. It can be calculated that the weight ratio of SnS_2 in the hybrid is about 85.17%. According to this ratio and the capacity of the graphene at 0.01–1.5 V *vs.* Li^+/Li (~390 mAh g^{-1}), it is

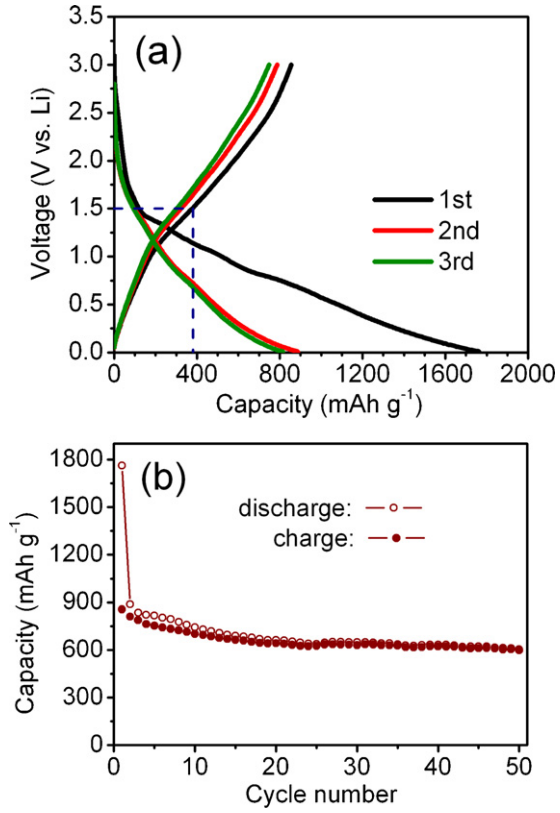

Fig. 6. (a) The first three charge and discharge curves of GNS obtained by a hydrothermal method employing GO and L-cys as the starting materials, and (b) cycling behavior at a current density of 100 mA g^{-1}.

Table 1
Composition of pure SnS_2 and FL-SnS_2/G hybrid prepared by solution-chemistry method.

Samples	Element (wt.%)				SnS_2 (wt.%)
	Sn	S	C	O	
SnS_2	64.84	35.16	–	–	100
FL-SnS_2/G	54.91	30.26	11.36	3.47	85.17

calculated that the attribution of FL-SnS_2 in the hybrid to specific capacity is up to 990 mAh g^{-1}. It is not considered that such a high capacity is attributed to only the SnS_2 nanosheets. According to the highest capacity of pure SnS_2 (645 mAh g^{-1}) reported by Seo et al. [17], it could be calculated that the capacity of the FL-SnS_2/G hybrid should be about 615 mAh g^{-1}, which is also lower than our measured value of 920 mAh $g^{-1}$of the FL-SnS_2/G hybrid. Therefore, such highly desirable electrochemical properties had to be the work of a robust composite structure and some synergistic interactions between layered SnS_2 and graphene. The presence of highly conductive graphene in the composite naturally increases the conductivity of the FL-SnS_2/G hybrid as a whole. The role of graphene here is to establish an interconnecting electronically conducting network allowing electron to percolate through the less-conductive SnS_2 phase. The interaction between the delocalized π-conjugation system of the graphene and the outer electrons of the S atoms in layered SnS_2 in proximal contact with the graphene facilitates rapid electron transfer in the electrode reaction. In addition, the 3D architectural FL-SnS_2/G hybrid with rough surface increases the contact area with the electrolyte and shortens the Li^+ diffusion paths in lithiation/delithiation processes.

In general capacity fading is caused by expansive volume excursions in the active electrode material during charging and discharging; leading to the pulverization of material and loss of electrical connectivity. The SnS_2 and FL-SnS_2/G electrodes were therefore examined by *ex situ* XRD and SEM and compared after 50 cycles of charge and discharge (Fig. 7). Comparing with the in situ XRD patterns (Fig. 5), it is found that the crystalline structures of two samples do not significantly change, but the peak intensity of Li_xSn decrease due to the decomposition themselves (Fig. 7a). To compare with the *ex situ* XRD and SEM, it can be seen that after 50 cycles, the crystalline structures of SnS_2 and SnS_2/G are basically same but their morphologies. Fig. 7b clearly shows the pulverization of the layered SnS_2 electrode after 50 cycles due to the aforementioned volume excursion effects. In stark contrast to this is the FL-SnS_2/G hybrid where pulverization was not detectable and the original composite structure was basically retained (Fig. 7c). Hence the presence of graphene contributed to buffering the volume changes in the active material and stabilizing thereby resulting in significantly improved cycling performance.

To further explain and better understand why FL-SnS_2/G electrode exhibits such a superior electrochemical performance compared to the layered SnS_2 electrode, electrochemical impedance measurements were performed after 5 cycles as shown in Fig. 8. The equivalent circuit model of the studied system is inserted in Fig. 8 according to the works reported by others [34]. R_e represents the internal resistance of the test battery, R_f and CPE_1 are associated with the resistance and constant phase element of SEI film, R_{ct} and CPE_2 are associated with the charge-transfer resistance and constant phase element of the electrode/electrolyte interface, Z_W represents Warburg impedance corresponding to the lithium-diffusion process. As shown in Fig. 8, the high frequency semicircle is corresponding to the resistance R_f and CPE_1 of SEI film, the semicircle in medium frequency region is assigned to the charge-transfer resistance R_{ct} and CPE_2 of electrode/electrolyte interface. The inclined line corresponds to the lithium-diffusion process within bulk of the electrode material. The kinetic differences of

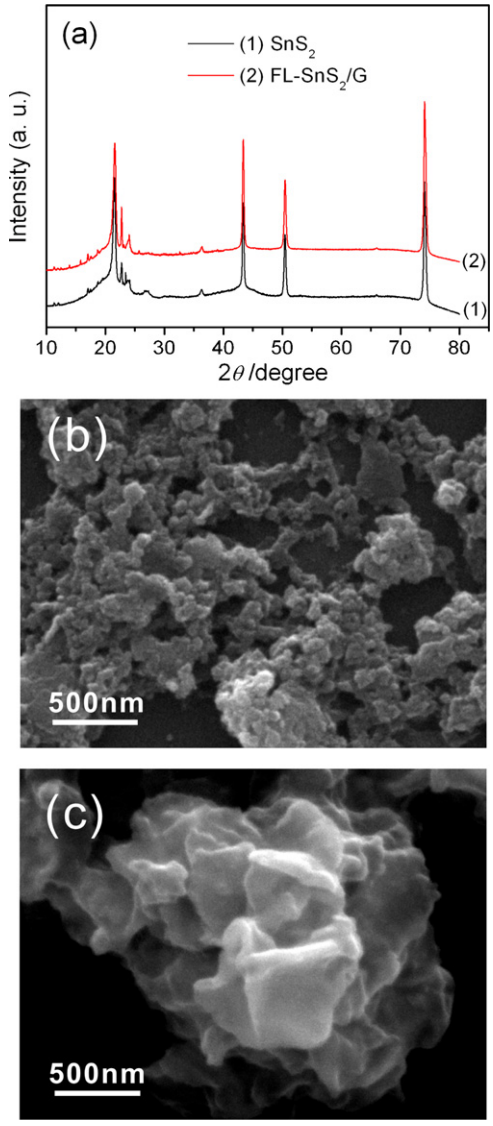

Fig. 7. (a) XRD patterns of (1) layered SnS_2 and (2) FL-SnS_2/G hybrid, and SEM images of (b) layered SnS_2 and (c) FL-SnS_2/G hybrid after 50 cycles at a current density of 100 mA g^{-1}.

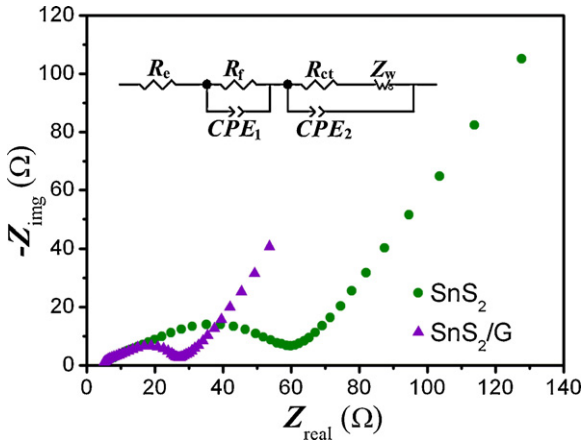

Fig. 8. Nyquist plots of the layered SnS_2 and FL-SnS_2/G electrodes; the inset shows equivalent circuit model of the studied system, CPE represent the constant phase element, $Z_{CPE} = \{Q(j\omega)^n\}^{-1}$, $0 \le n \le 1$.

Table 2
Impedance parameters derived using equivalent circuit model for SnS_2 and FL-SnS_2/G electrodes.

Electrodes	R_e (Ω)	R_f (Ω)	Q_1 (μF)	R_{ct} (Ω)	Q_2 (μF)
SnS_2	5.473	11.91	51.6	34.79	65.1
FL-SnS_2/G	4.369	8.99	91.4	10.37	324.0

FL-SnS_2/G and layered SnS_2 electrodes were further investigated by modeling electrochemical impendence spectra based on the modified Randles equivalent circuit [35]. The fitted impedance parameters are listed in Table 2. The values of R_f and R_{ct} of the FL-SnS_2/G electrode are 8.99 and 10.37 Ω respectively, which are significantly lower than those of the layered SnS_2 electrode (11.91 and 34.79 Ω). The fact confirms that the incorporation of graphene can not only preserve the high conductivity of the FL-SnS_2/G hybrid, but also greatly enhance rapid electron transport during electrochemical lithium insertion/extraction process, resulting in significant improvement in the electrochemical performances of the FL-SnS_2/G hybrid.

4. Conclusions

In summary, the structural compatibility between the layered structural SnS_2 and graphene suggested the possibility to design a new composite as LIB anode material without the deficiency of most graphene composites with metal oxides, Sn or Si. The novel anode material in the form of a FL-SnS_2/G hybrid was synthesized by a facile L-cys-assisted solution-chemistry method. It delivered a high specific capacity (920 mAh g^{-1}) with excellent cycling stability and high-rate capability. The impressive electrochemical performance may be attributed to a robust composite architecture that withstands the stress of cycling; and complementarity and synergistic interactions between the layered SnS_2 and graphene. The encouraging experimental results suggest that the new FL-SnS_2/G hybrid has great potential for the LIBs for demanding applications.

Acknowledgments

This work was supported by the Natural Science Foundation of China (21173190), the Program for International Science and Technology Cooperation Projects of China (the 8th Science and Technology Cooperation Projects of China-Singapore, S2012GR0025), the Program from Science and Technology Department of Zhejiang Province (2011G210024), the Research Fund for the Doctoral Program of Higher Education of China (20050335086), the Zhejiang Provincial Natural Science Foundation of China (Y4100119), and 973 Fundamental Research Program from the Ministry of Science and Technology of China (2010CB635116).

References

[1] M. Winter, R.J. Brodd, Chem. Rev. 104 (2004) 4245–4269.
[2] A.K. Geim, K.S. Novoselov, Nat. Mater. 6 (2007) 183–191.
[3] E. Yoo, J. Kim, E. Hosono, H. Zhou, T. Kudo, I. Honma, Nano Lett. 8 (2008) 2277–2282.
[4] B. Wang, X.L. Wu, C.Y. Shu, Y.G. Guo, C.R. Wang, J. Mater. Chem. 20 (2010) 10661–10664.
[5] M. Pumera, Chem. Rec. 9 (2009) 211–223.
[6] G.X. Wang, X.P. Shen, J. Yao, J. Park, Carbon 47 (2009) 2049–2053.
[7] Y.Q. Sun, Q.O. Wu, G.Q. Shi, Energ. Environ. Sci. 4 (2011) 1113–1132.
[8] L.S. Zhang, L.Y. Jiang, H.J. Yan, W.D. Wang, W. Wang, W.G. Song, Y.G. Guo, L.J. Wan, J. Mater. Chem. 20 (2010) 5462–5467.
[9] J.Z. Wang, C. Zhong, S.L. Chou, H.K. Liu, Electrochem. Commun. 12 (2010) 1467–1470.
[10] G.X. Wang, B. Wang, X.L. Wang, J. Park, S.X. Dou, H. Ahn, K. Kim, J. Mater. Chem. 19 (2009) 8378–8384.
[11] J. Yao, X.P. Shen, B. Wang, H.K. Liu, G.X. Wang, Electrochem. Commun. 11 (2009) 1849–1852.

[12] J.K. Lee, K.B. Smith, C.M. Hayner, H.H. Kung, Chem. Commun. 46 (2010) 2025–2027.
[13] I. Lefebvre, M. Lannoo, M.E. Moubtassim, J.O. Fourcade, J.C. Jumas, Chem. Mater. 9 (1997) 2805–2814.
[14] J. Morales, C. Perezvicente, J.L. Tirado, Solid State Ionics 51 (1992) 133–138.
[15] T. Brousse, R. Retoux, U. Herterich, D.M. Schleich, J. Electrochem. Soc. 145 (1998) 1–4.
[16] J.G. Lee, D. Son, C. Kim, B. Park, J. Power Sources 172 (2007) 908–912.
[17] J.W. Seo, J.T. Jang, S.W. Park, C.J. Kim, B.W. Park, J.W. Cheon, Adv. Mater. 20 (2008) 4269–4273.
[18] C.X. Zhai, N. Du, H. Zhang, D.R. Yang, Chem. Commun. 47 (2011) 1270–1272.
[19] C.R. German, P. Santiago, J.A. Ascencio, U. Pal, M. Perez-Alvarez, L. Rendon, D. Mendoza, J. Phys. Chem. B 109 (2005) 17488–17495.
[20] W.S. Hummers, R.E. Offeman, J. Am. Chem. Soc. 80 (1958) 1339.
[21] H.L. Wang, L.F. Cui, Y.A. Yang, H.S. Casalongue, J.T. Robinson, Y.Y. Liang, Y. Cui, H.J. Dai, J. Am. Chem. Soc. 132 (2010) 13978–13980.
[22] Y.X. Xu, K.X. Sheng, C. Li, G.Q. Shi, ACS Nano 4 (2010) 4324–4330.
[23] Z.S. Wu, W.C. Ren, L. Wen, L.B. Gao, J.P. Zhao, Z.P. Chen, G.M. Zhou, F. Li, H.M. Cheng, ACS Nano 4 (2010) 3187–3194.
[24] S.Q. Chen, P. Chen, M.H. Wu, D.Y. Pan, Y. Wang, Electrochem. Commun. 12 (2010) 1302–1306.
[25] J. Xiao, D.W. Choi, L. Cosimbescu, P. Koech, J. Liu, J.P. Lemmon, Chem. Mater. 22 (2010) 4522–4524.
[26] H.S. Kim, Y.H. Chung, S.H. Kang, Y.E. Sung, Electrochim. Acta 54 (2009) 3606–3610.
[27] T.J. Kim, C. Kirn, D. Son, M. Choi, B. Park, J. Power Sources 167 (2007) 529–535.
[28] C. Julien, C. PerezVicente, Solid State Ionics 89 (1996) 337–343.
[29] K. Chang, W.X. Chen, L. Ma, H. Li, H. Li, F.H. Huang, Z.D. Xu, Q.B. Zhang, J.Y. Lee, J. Mater. Chem. 21 (2011) 6251–6257.
[30] W.L. Yao, J. Yang, J.L. Wang, Y. Nuli, J. Electrochem. Soc. 155 (2008) A903–A908.
[31] J.T. Zai, K.X. Wang, Y.Z. Su, X.F. Qian, J.S. Chen, J. Power Sources 196 (2011) 3650–3654.
[32] S. Liu, X.M. Yin, L.B. Chen, Q.H. Li, T.H. Wang, Solid State Sci. 12 (2010) 712–718.
[33] K. Chang, W.X. Chen, ACS Nano 5 (2011) 4720–4728.
[34] P. Guo, H.H. Song, X.H. Chen, Electrochem. Commun. 11 (2009) 1320–1324.
[35] S.B. Yang, X.L. Feng, L.J. Zhi, Q.A. Cao, J. Maier, K. Mullen, Adv. Mater. 22 (2010) 838–842.